Title

Covariability of zooplankton gradients with glider-detected density fronts in the Southern California Current System

Authors

Powell, Jesse R
Ohman, Mark D

Publication Date

2015-02-01

DOI

10.1016/j.dsr2.2014.04.002

Peer reviewed

Deep-Sea Research II ∎ (∎∎∎∎) ∎∎∎–∎∎∎

Contents lists available at ScienceDirect

Deep-Sea Research II

journal homepage: www.elsevier.com/locate/dsr2

Covariability of zooplankton gradients with glider-detected density fronts in the Southern California Current System

Jesse R. Powell *, Mark D. Ohman

California Current Ecosystem LTER site, Scripps Institution of Oceanography, University of California, San Diego, La Jolla, CA 92093-0218, USA

ARTICLE INFO

Keywords:
Oceanic fronts
Zooplankton
Foraging behavior
Eastern boundary currents
Acoustic backscatter

ABSTRACT

Fronts represent sharp boundaries between water masses, but seasonal and interannual variation in their occurrence and effects on the distributions of pelagic organisms are poorly understood. This study reports results from six years of ocean front observations (2006–2011) along two transect lines across the Southern California Current System (SCCS) using autonomous *Spray* ocean gliders. During this time, 154 positive near-surface density fronts were identified within 124 completed transects consisting of nearly 23,000 vertical profiles. The incidence of surface density fronts showed distinct seasonality along line 80 off Pt. Conception, with fewer fronts occurring during winter months and more numerous fronts in the nearshore and during spring, summer and fall. On line 90, fronts were the least common nearshore and most frequent in a transitional region offshore. Horizontal density gradients in the surface layer (0–50 m) were significantly correlated with horizontal gradients in surface layer Chlorophyll-*a* (Chl-*a*) fluorescence, as well as with mean volume backscatter (MVBS) recorded by a 750 kHz acoustic Doppler profiler. Density fronts were not only zones of rapidly changing phytoplankton and zooplankton biomass concentrations, but also more likely to be zones of enhanced acoustic backscatter and Chl-*a* fluorescence than regions flanking the fronts. MVBS and Chl-*a* gradients were significantly correlated with gradients in other hydrographic variables such as temperature, salinity, and spiciness, and weakly with cross-track current velocity, though density gradients remained the single best predictor of strong MVBS and fluorescence gradients. Large mobile predators foraging in the vicinity of such features could locate habitat with higher zooplankton biomass concentrations up to 85% of the time by traveling up local density gradients (*i.e.*, toward rather than away from denser surface waters). We discuss implications of these results in the context of long-term trends in ocean fronts in the SCCS.

1. Introduction

Fronts delineate boundaries between different water masses or parcels, and consequently are often areas characterized by strong horizontal gradients in hydrographic properties such as density, temperature, or salinity (Legeckis, 1978; Sournia, 1994). While there are several categories of fronts, generated under a variety of conditions (*e.g.*, estuarine fronts, river plume fronts, tidal fronts, shelf-break fronts, among others), this paper examines open ocean fronts in the Southern California Current System (SCCS) and their role in shaping distributions of zooplankton and phytoplankton biomass.

Fronts have long been considered locations of special ecological significance for zooplankton (Boucher et al., 1987; Lefevre, 1986). Both modeling and field studies have demonstrated that primary productivity can be significantly elevated at fronts due to transient vertical mixing events (Claustre et al., 1994; Franks and Walstad, 1997). Enhanced nutrient availability can enable growth of larger phytoplankton such as diatoms (Claustre et al., 1994; Landry et al., 2012; Taylor et al., 2012) that are more readily grazed by mesozooplankton. Both the composition and biomass of zooplankton assemblages can change abruptly across fronts (Mackas et al., 1991; Ohman et al., 2012). Increased copepod egg production rates (Smith and Lane, 1991) and nauplii per copepod (Ohman et al., 2012) have been observed at phytoplankton-rich fronts. A study of the Ensenada Front (Haury et al., 1993), a semi-recurrent frontal feature west of San Diego, found 3–4 fold higher zooplankton displacement volumes on the cool (North) side of the front where primary productivity was also elevated. Moser and Smith (1993) found distinct assemblages of fish larvae on either side of the same front. Fronts may also be sites of elevated abundances of mobile predators such as large fish (Fiedler and Bernard, 1987; Podesta et al., 1993), marine mammals (Bost et al., 2009; Tynan et al., 2005), and seabirds (Ainley et al., 2009; Kai et al., 2009). GPS-tracking studies have confirmed that seabirds can actively target and follow open ocean fronts (Kai et al., 2009).

* Corresponding author.
E-mail addresses: jesse@jessepowell.info (J.R. Powell), mohman@ucsd.edu (M.D. Ohman).

http://dx.doi.org/10.1016/j.dsr2.2014.04.002
0967-0645/

Our understanding of zooplankton ecology at fronts is limited, however, because fronts are dynamic and often inadequately sampled by conventional technologies. In addition, advection along the length of a single front can vary rapidly from convergent to divergent, and from upwelling to downwelling in response to local winds (D'Asaro et al., 2011; Franks and Walstad, 1997), frontal meanders (Bower, 1991), or secondary circulation (D'Asaro et al., 2011), leading to changes in nutrient supply, light penetration, and localized accumulation and dispersal of plankton. Ocean fronts can persist on varying timescales ranging from days to weeks, making prediction of zooplankton and phytoplankton responses to altered environmental conditions at fronts difficult. Furthermore, zooplankton are not passive particles and can alter their swimming or vertical migration behavior in response to changing physical conditions. Varying vertical migration behaviors can lead to markedly different zooplankton densities at both convergent and divergent flows (Franks, 1992).

Mechanisms leading to the development of plankton gradients or localized accumulation zones can be divided into four general categories. Plankton can accumulate due to convergent flows. Horizontal shear or stirring can bring two water parcels containing different plankton concentrations in close proximity. Altered *in situ* plankton growth or predation can increase or decrease local densities. Lastly, changes in zooplankton swimming and vertical migration behavior can interact with local advection, leading to the local accumulation or dispersal of zooplankton. Regardless of which mechanism dominates in specific cases, however, the front-seeking behavior observed in mobile predators (Kai et al., 2009) suggests that zooplankton accumulation at fronts is not uncommon, and that fronts, while limited in areal extent, may play a disproportionate role in predator behavior as well as zooplankton reproduction, growth, and mortality.

While previous studies suggest that fronts may be important in structuring the distribution, productivity and behavior of zooplankton within the CCS, each is based on observations of limited duration of a single front for which shipboard sampling was possible. To assess the more general significance of these spatial discontinuities, it is necessary to observe a variety of fronts over an extended period, throughout different seasons, and across a broad area. Autonomous ocean gliders represent a means to extend our observational capabilities when studying ocean fronts. Since 2006, *Spray* gliders (Davis et al., 2008; Ohman et al., 2013) have been deployed nearly continuously along two cross-shore ocean transects, lines 80 and 90 within the SCCS (Fig. 1). Lines 80 and 90 are part of the CalCOFI sampling grid that has been sampled by ship for 65 years, and since 2004 have been sampled as part of the California Current Ecosystem–Long Term Ecological Research (CCE–LTER) program (http://cce.lternet.edu). More recently, two interdisciplinary moorings have been established along line 80 (Ohman et al., 2013). Together, lines 80 and 90 span most of the range of oceanographic conditions found within the SCCS.

Here we address the following specific questions regarding the covariability of ocean fronts and zooplankton and phytoplankton gradients within the SCCS along lines 80 and 90. Do the occurrence and spatial distribution of ocean fronts show distinct seasonal and cross-shore patterns? Do gradients in biotic properties consistently covary with gradients in physical ocean properties? Are ocean fronts more likely to be zones of plankton accumulation than non-frontal regions?

2. Methods

2.1. Study area and duration

The data included in this analysis span from October 2006 to July 2011, though gliders continue to be deployed at time of publication. During this period, gliders were deployed nearly continuously along lines 80 and 90 of the CalCOFI sampling area (Fig. 1). Gliders traveling along the two lines traverse from about 20 km off the coast to a maximum 370 km (line 80) and 585 km (line 90) offshore. A total of 124 transects, 62 on each line, were completed during the study period, comprising 22,942 vertical profiles.

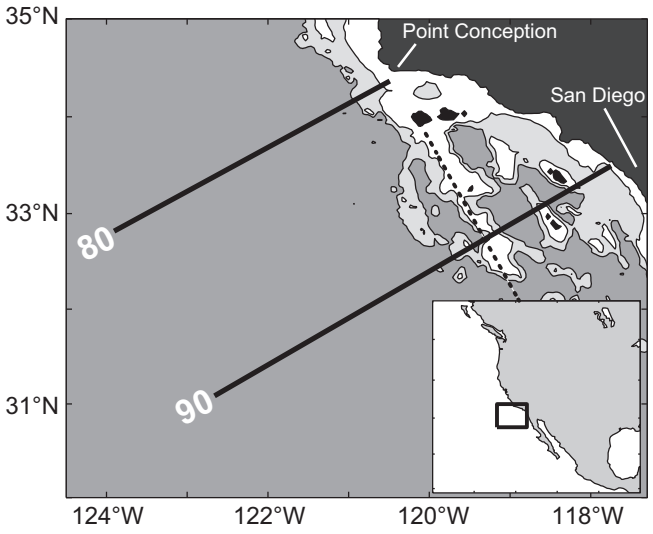

Fig. 1. CCE–LTER *Spray* glider transect lines 80 and 90. Contours on main illustration indicate bottom depth (white = 0–500 m; light gray = 500–1000 m; dark gray ≥ 1000 m). Dotted line indicates Santa Rosa-Cortes Ridge. Inset shows location off the West Coast of North America.

Line 80, extending west–southwest from Point Conception, is often marked by cold, upwelled waters close to the coast, and is bounded to the west by the fresher and somewhat warmer core of the equatorward-flowing California Current (CC) proper. The major currents, including the CC, the California Undercurrent (CUC), and the Inshore Countercurrent (ICC), are often intensified compared to line 90, with more compact, faster flowing cores along line 80. In contrast, line 90 is often influenced by warmer, more subtropical waters intruding from the South and West. Maximum current velocities tend to be reduced as well. Bottom depth along line 80 increases nearly monotonically, and rapidly with distance offshore across the continental slope. Line 90, on the other hand, crosses several undersea ridges and sea mounts as it traverses the Southern California Bight and region offshore. *Spray* glider studies along line 90 suggest that the submarine Santa Rosa-Cortes Ridge is a site of enhanced mixing (Johnston and Rudnick, this issue). The differing bathymetries of lines 80 and 90 may influence the mechanisms by which fronts form along these two lines.

2.2. Spray glider and instrument payload

The *Spray* glider (Sherman et al., 2001) is a buoyancy-controlled autonomous underwater vehicle capable of conducting profiles to 1000 m depth for up to 4 months at a time as presently configured. The vehicle profiles in a sawtooth pattern, traveling at an average speed of 25 cm s^{-1} through water, at an angle of 17° from the horizontal. For this study, gliders descended to a maximum depth of 500 m, or to within approximately 5 m from the bottom in shallower waters. Sensors were activated and data recorded only on the upward profiles. At the end of each profile, the glider surfaces, establishes a GPS fix, and uploads data *via* the Iridium satellite system. The glider follows a pre-programmed mission along a transect until it receives instructions to change operations. In waters deeper than 500 m, the glider will complete a profile cycle every 3 h, on average, with an average spacing between profiles of 3 km.

Please cite this article as: Powell, J.R., Ohman, M.D., Covariability of zooplankton gradients with glider-detected density fronts in the Southern California Current System. Deep-Sea Res. II (2014), http://dx.doi.org/10.1016/j.dsr2.2014.04.002

The *Spray*'s instrument payload during this study included a Seabird 41CP Conductivity–Temperature–Depth (CTD) sensor, a mini-Seapoint Chlorophyll-*a* fluorometer (mini-SCF), and a Sontek 750-kHz, 3-beam Acoustic Doppler Profiler (ADP). During sampling, seawater is continuously pumped through the CTD and the fluorometer to maintain a constant flow rate past the sensors. Biofouling is inhibited by pumping seawater through a biocide-treated intake tube.

The Seapoint fluorometers used in this study had a central excitation peak of 470 nm and an emission peak of 685 nm. Fluorometers were regularly calibrated between deployments using a standard set of dilutions of pure chlorophyll-*a* (Sigma Life Sciences) dissolved in 90% acetone. Each Chl-*a* standard was first loaded into a 13 mm diameter borosilicate round cuvette, and then placed within a machined cuvette-holder that held the standard at a fixed distance from the optical surfaces of the fluorometer. For each calibration, a slope value (μg Chl-*a* L^{-1} V^{-1}) was determined from a regression of recorded voltage with dissolved Chl-*a* concentrations. Regular calibration enabled intercomparison of data from the same sensor during different deployments, and also comparability of data recorded by different sensors. The fluorometer response recorded during deployments is reported here in standardized Chl-*a* fluorescence units (SFU), where one SFU is defined as the measured fluorescence signal (V) from 10 μg L^{-1} of Chl-*a* dissolved in 90% acetone (cf., previously reported as Dissolved Chlorophyll Fluorescence Equivalents (DCFE) in Davis et al. (2008)). *in vivo* fluorescence data were converted into SFU by multiplying the recorded voltages by the mean slope value determined from pre- and post-deployment calibrations. For the fluorometers used in this study, one SFU corresponds very approximately to 2 μg Chl-*a* L^{-1} by comparison with phytoplankton analyzed from the Scripps pier. While SFU data cannot be directly converted into *in situ* Chl-*a* concentrations, SFU data do provide useful measures of standardized Chl-*a* fluorescence that are comparable across all instruments.

The Sontek *Spray* ADP is mounted on the glider such that it points directly down during glider ascent, so that each of the three beams has a slant angle of 25° from vertical. Each beam has a 3 dB beam width of 2° and samples the sample volume of water. Both current velocity and acoustic backscatter (ABS) data from the ADP are recorded upon ascent in five 4-m vertical range bins so that vertical resolution of the completed profile is 4 m. The backscatter measured by the ADP is reported in acoustic counts, which is the digitized output from a log–linear amplifier. Regular calibration of each ADP using a standard tungsten-carbide target suspended in a test pool revealed an average difference in ABS recorded by an individual ADP across multiple deployments of 2.5 dB, and an average difference between different ADP instruments of 3 dB; these differences are much smaller than the magnitude of the differences analyzed here. Furthermore, the calculation of spatial gradients is not sensitive to such differences. The recorded ABS is then converted into Volume Backscatter, S_v, using the sonar equation $S_v = RL - SL + 2TL - 10\log_{10} V$, where Receiver Level (RL) is the recorded ABS in dB, Source Level (SL) in decibels is empirically determined during instrument calibration, Transmission Loss (TL) is equivalent to $20\log_{10} R + \alpha R$, where R is the range in meters to the midpoint of the bin and α is the sound attenuation coefficient (dB m^{-1}), and V is the volume in cubic meters. Volume backscatter measurements are averaged to yield Mean Volume Backscatter (MVBS).

Previous work established that recorded ABS is proportional to the log of net-collected zooplankton biomass in the vicinity of the ADP (Powell and Ohman, 2012). ZooScan image analysis of zooplankton in net samples showed that ABS was most closely related to zooplankton with an equivalent circular diameter $\geq$ 1.6 mm, approximately the acoustic wavelength emitted by the transducer. It is important to note, however, that the method used to calculate relative MVBS in Powell and Ohman (2012) relied on a different formulation of the sonar equation (SonTek, 1997). The standard sonar equation presented here (Medwin and Clay, 1998) includes a 10 $\log_{10} V$ term rather than a 10 $\log_{10}$ PL term (where PL is the acoustic pulse length), which permitted comparison of backscatter from different range cells. Applying this method to the data from Powell and Ohman (2012) did not alter any of the results or conclusions of that paper.

2.3. Glider data processing

Data from each glider deployment were downloaded from the glider's flash memory upon glider recovery and imported into MATLAB for quality assurance and control. Bad data, as determined by processing scripts or visual inspection, were excluded from further analysis. The data from all glider deployments were then harvested into a master MATLAB dataset and grouped by transect. Only data from complete transects, where the glider completed 90% or more of its intended trackline, were included in the analysis. Variables included in this study include temperature, salinity, density, Chl-*a* fluorescence (as SFU), salinity on potential isopycnals, which has the same information as spice (Flament, 2002), cross-track and along-track current velocity, and MVBS. For each profile within a given transect, all data were vertically averaged into 5-m bins. Most analyses in this study examine changes in measured variables in a near-surface layer from 0 to 50 m.

2.4. Horizontal time binning, gradient calculation, enhancement index and front detection.

Comparing glider data from one profile to the next is confounded by diel periodicity in biological signals (in the case of MVBS and *in vivo* fluorescence data), and by the influence of internal tides and inertial motions (in the case of hydrographic variables). Diel vertical migrations (DVM) by zooplankton and micronekton dramatically influence the total biomass concentrations observed in daytime surface waters. Similarly, fluorescence measured in surface waters is affected by the daytime decrease in Chl-*a* fluorescence due to non-photochemical quenching, and to daytime photoprotective strategies employed by phytoplankton (Cullen and Lewis, 1995). Thus, searching for biological fronts by directly comparing surface MVBS or Chl-*a* fluorescence from adjacent nighttime and daytime profiles is not possible. Furthermore, the calculation of gradients in hydrographic variables (*i.e.*, density, temperature, salinity, *etc.*) is confounded by internal tides and waves which can vertically displace physical features such as the thermocline from dive to dive. For these reasons, both physical and biological data were smoothed prior to use by averaging observations within a 24-h period. Horizontal gradient values (Fig. 2A and B) are defined as the difference between averages of properties from the 24 h periods before and after the glider reached a location, divided by the distance traveled. By definition here, a gradient is the onshore average minus the offshore average.

The enhancement index (Fig. 2C and D) of a given dive measures whether waters within a 24 h block of dives just inshore of the given dive exhibit increased (positive), decreased (negative), or neither increased or decreased (zero) enhancement of average MVBS or Chl-*a* fluorescence compared to the two flanking 24 h blocks. For a given dive location, the center block ("Box2") represents the average of MVBS or Chl-*a* data recorded in the 24 h period just inshore of the dive, and the two flanking blocks ("Box1" and "Box3" in Fig. 2C) represent the average data from the flanking offshore and inshore 24 h periods, respectively. The enhancement index, $EI = K(|Box2 - Box1| + |Box2 - Box3|)$, where vertical lines indicate absolute values. $K = 1$ if Box2 is greater than

Please cite this article as: Powell, J.R., Ohman, M.D., Covariability of zooplankton gradients with glider-detected density fronts in the Southern California Current System. Deep-Sea Res. II (2014), http://dx.doi.org/10.1016/j.dsr2.2014.04.002

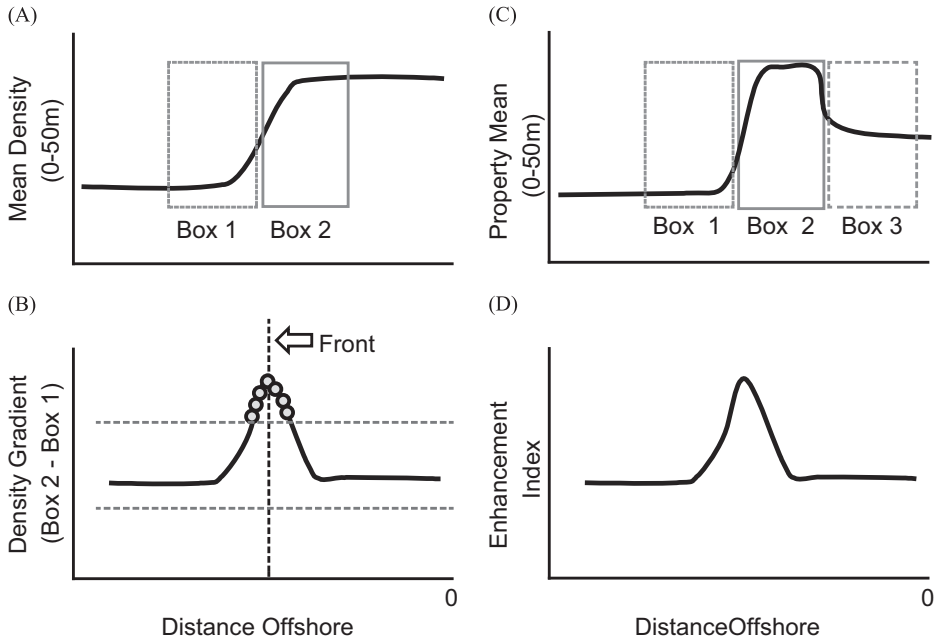

Fig. 2. Schematic diagrams illustrating the definition of gradients, fronts, and enhancement indices. (A) Gradients are calculated by subtracting the mean of near-surface density values recorded during a 24 h block of dives located offshore (Box1) of a given dive from the 24 h average inshore of a dive (Box2). (B) Fronts (vertical dashed line) are picked from contiguous run of dives (black circles) having gradients higher than the 95th or lower than the 5th percentile (horizontal dotted lines) of density gradients. (C and D) The enhancement index (EI) is defined as $EI = K(|Box2 - Box1| + |Box2 - Box3|)$, where vertical lines indicate absolute value, and $K = 1$ if Box2 is greater than Box1 and Box3, $K = -1$ if Box2 is less than Box1 and Box3, or $K = 0$ otherwise.

Box1 and Box3, $K = -1$ if Box2 is less than Box1 and Box3, otherwise $K = 0$. Dives with horizontal density gradient values greater than the 95th percentile or less than the 5th percentile are flagged as potential "positive" density fronts (*i.e.*, inshore density > offshore density) or "negative" density fronts (*i.e.*, inshore density < offshore density), respectively. When more than one contiguous dive is flagged as a potential front, the dive with the maximum (minimum) gradient value within the contiguous run of dives is denoted as a positive (negative) density front. Other front types, identified with any of the other glider-measured variables (*e.g.*, thermal, salinity, or MVBS fronts), are identified in an identical manner. Our analysis focuses primarily on positive density fronts because they were consistently much steeper gradients than the negative density fronts along both lines 80 and 90.

3. Results

3.1. Coincident biological and physical structures observed in glider sections

Visual inspection of glider transects reveals that regions of increased horizontal gradients in biotic properties such as acoustic backscatter and Chl-*a* fluorescence are often, but not always, associated with oceanic density fronts. In an example glider section (Fig. 3), a sharp density front ~185 km offshore is colocated with corresponding fronts in temperature, salinity, MVBS, and modest changes in cross-track and along-track current velocities in the top 50 m. There is a 9 dB drop in mean MVBS in the top 50 m across the density front (Fig. 3F) that could correspond to an 8-fold change in biomass. This particular front does not manifest a corresponding front in Chl-*a* fluorescence, indicating that the relationship between physical and biological properties at fronts varies, and that zooplankton and phytoplankton may be, at times, independently influenced by frontal conditions, or that interactions between zooplankton and phytoplankton at fronts also act to structure abundance and biomass.

3.2. Glider-detected oceanic density fronts along lines 80 and 90

A total of 81 positive density fronts along line 80 and 73 positive density fronts along line 90 were identified by the front-detection criteria. Lines 80 and 90 differed in the distribution of their respective fronts in terms of location (distance offshore) and day of the year (Fig. 4). There were relatively few fronts in the offshore portion of transects along line 80, with most fronts found within 150 km of the shore. There were also relatively few fronts during the first 90 days of the year. A comparison of density gradients at fronts along lines 80 and 90 indicated that gradient magnitudes were significantly stronger along line 80 ($p < 0.05$, Mann–Whitney U test). Tests of the effect of season upon front incidence and front strength (as measured by the magnitude of the along-track density gradient) for lines 80 and 90 (Fig. 5A–D) confirmed the seasonal patterns suggested in Fig. 4. There were significantly fewer fronts in winter for line 80 ($p < 0.05$, binomial test with the Bonferroni correction to correct for multiple comparisons). The magnitudes of density gradients at fronts did not vary significantly by season for lines 80 and 90 (Fig. 5C and D; $p > 0.05$, Kruskal–Wallis).

To test the influence of distance offshore upon front incidence and front strength, fronts along line 80 and along 90 were classified into one of three distance categories: near-shore (0–150 km), transitional (151–300 km), and offshore (> 300 km from shore). There were significantly more fronts than average inshore and significantly fewer fronts in the transitional region and far offshore along line 80 (Fig. 5E; $p < 0.01$, binomial test with the Bonferroni correction). In contrast, along line 90 there were significantly fewer fronts near-shore, and significantly more in the transitional region (Fig. 5F; $p < 0.01$, binomial test with the Bonferroni correction). The magnitude of density gradients at fronts along lines 80 and 90 did not vary significantly with distance offshore (Fig. 5G and H; $p > 0.10$, Kruskal–Wallis).

The median distance of fronts from shore did not differ significantly by bi-monthly time periods (Fig. 6, $p > 0.05$).

Please cite this article as: Powell, J.R., Ohman, M.D., Covariability of zooplankton gradients with glider-detected density fronts in the Southern California Current System. Deep-Sea Res. II (2014), http://dx.doi.org/10.1016/j.dsr2.2014.04.002

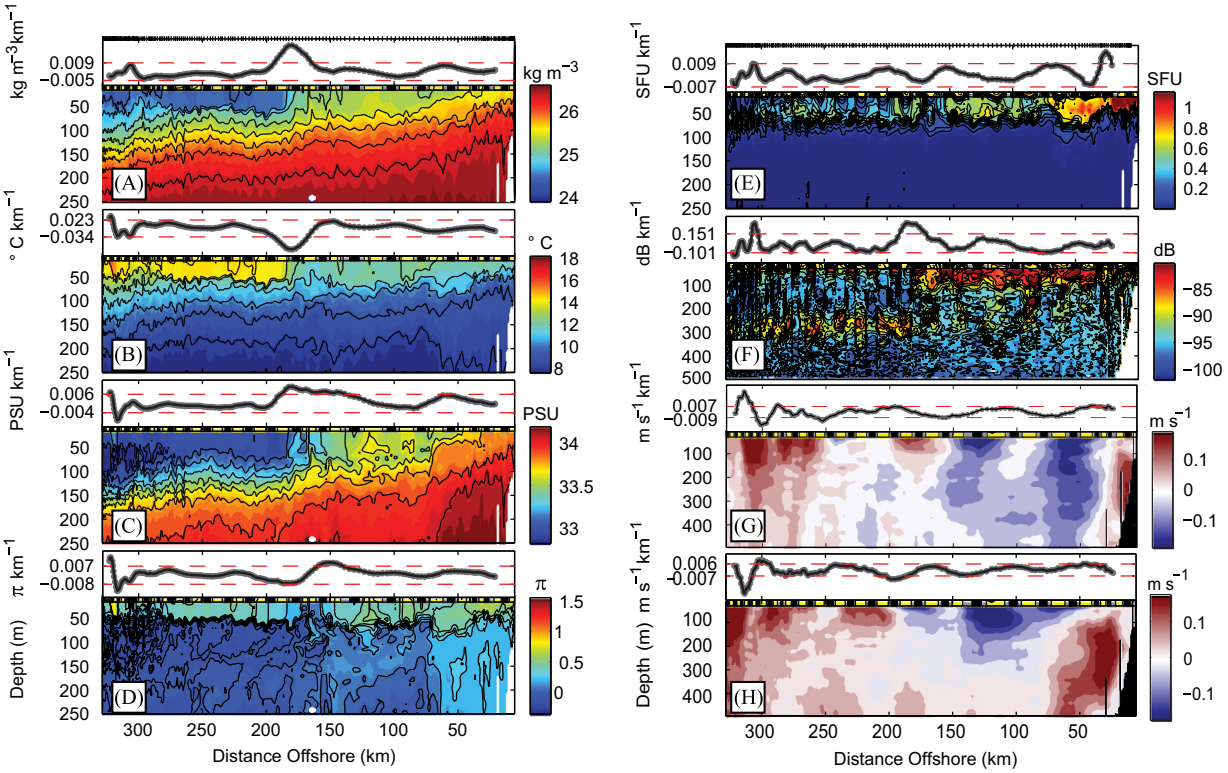

Fig. 3. Glider sections along line 80 showing (A) density (σ_0), (B) temperature (°C), (C) salinity, (D) spiciness (π), (E) Chl-*a* (SFU), (F) acoustic backscatter (MVBS, dB), (G) cross-track current velocity (m s^{-1}), and (H) along-track current velocity (m s^{-1}). Each panel shows a vertical section of a variable (color contours), beneath the near-surface (0–50 m) horizontal gradient of that variable (dark line). Tick marks at the top of panels (A and E) show the location of glider dives. Black, gray, and yellow bars at the top of each section plot indicate night, twilight, and day periods, respectively. Dashed red lines in each gradient plot indicate the value of the 5th and 95th percentiles of the gradient for the entire dataset.

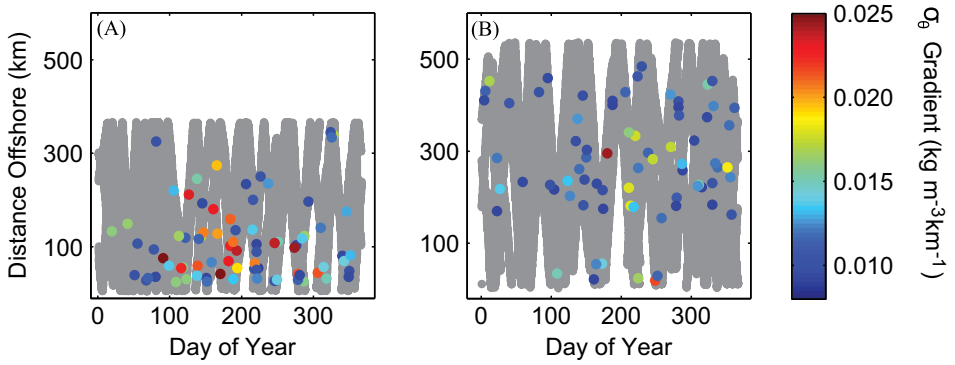

Fig. 4. Seasonal and cross-shore distribution of density fronts along (A) line 80, and (B) line 90. Gray dots indicate the distribution of all dives from October 2006 to November 2011. Colored dots show dives that were identified as positive density fronts. Color scale indicates the magnitude of the horizontal density gradient.

3.3. *Covariability of density gradients and acoustic backscatter gradients*

Density gradients and MVBS gradients covaried during the study period. There is a significant rank correlation between horizontal gradients in density and horizontal gradients in MVBS (Fig. 7A and C) for both line 80 ($r_s=0.42$, $p<0.001$) and line 90 ($r_s=0.43$, $p<0.001$). Furthermore, the MVBS gradients at dives identified as density fronts are significantly higher than the MVBS gradients at dives not associated with density fronts (Fig. 7B and D). While the relationship between density and MVBS gradients is significant, it also varies. Not all dives identified as positive density fronts also exhibit strong, positive MVBS gradients, indicating that other factors besides density gradient strength influence the distribution of zooplankton gradients.

Chlorophyll-*a* fluorescence gradients also show a significant, positive rank correlation with density gradients (Fig. 8), though not as strong (line 80: $r_s=0.31$, $p<0.001$; line 90: $r_s=0.36$, $p<0.001$). Interestingly, the correlation between MVBS gradients and Chl-*a* fluorescence gradients is weaker (line 80: $p<0.001$, $r_s=0.23$; line 90: $p<0.001$, $r_s=0.26$) than that of the density gradient with either the MVBS gradient or Chl-*a* fluorescence gradient, indicating that high horizontal gradients in Chlorophyll-*a* are a worse predictor of zooplankton distributions than the presence of high horizontal gradients in density.

Calculation of the correlations in Figs. 7 and 8 for each season (winter, spring, summer, and fall) independently showed that MVBS and Chl-*a* fluorescence gradients were positively correlated with density gradients in all seasons ($p<0.001$; data not shown).

Please cite this article as: Powell, J.R., Ohman, M.D., Covariability of zooplankton gradients with glider-detected density fronts in the Southern California Current System. Deep-Sea Res. II (2014), http://dx.doi.org/10.1016/j.dsr2.2014.04.002

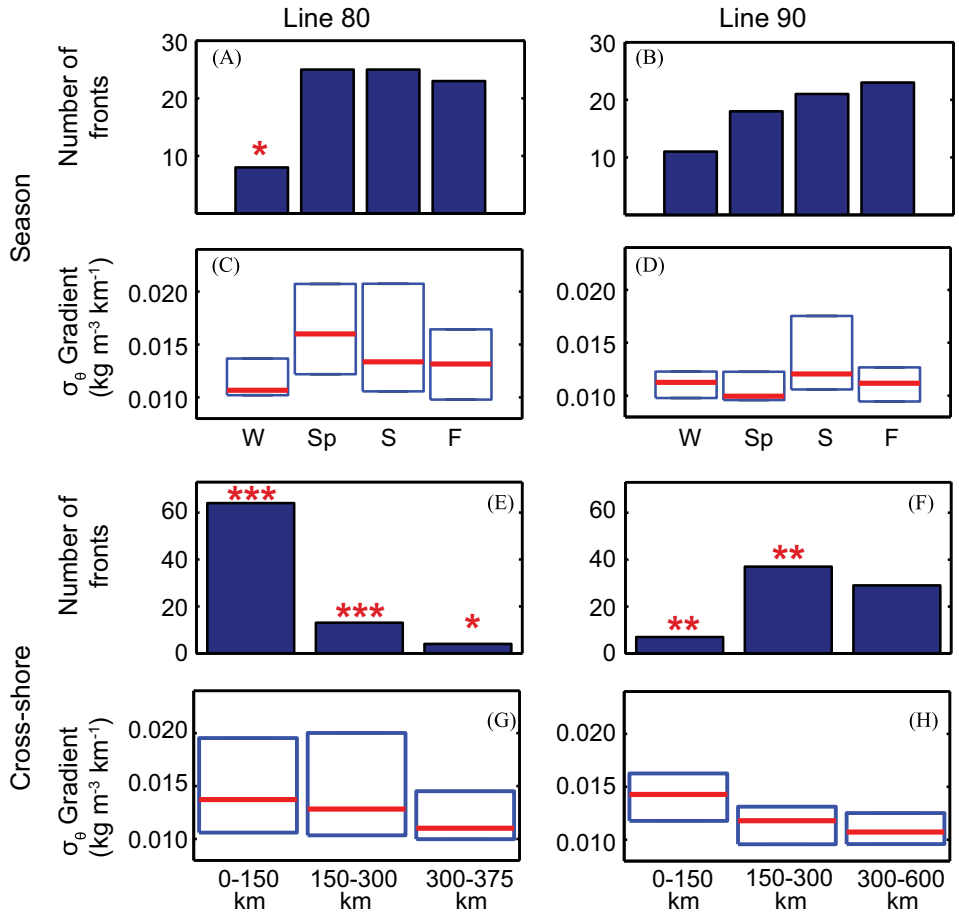

Fig. 5. Incidence and gradient strength of positive density fronts along lines 80 and 90, by season and distance offshore. The upper and lower bounds of boxplots mark the 75th and 25th percentile values of the density gradients, respectively, and the thick horizontal line marks the median gradient value. Asterisks in bar charts indicate significantly increased or decreased front incidence than the average for that line (*$p < 0.05$, **$p < 0.01$, and ***$p < 0.001$, binomial test with Bonferroni correction).

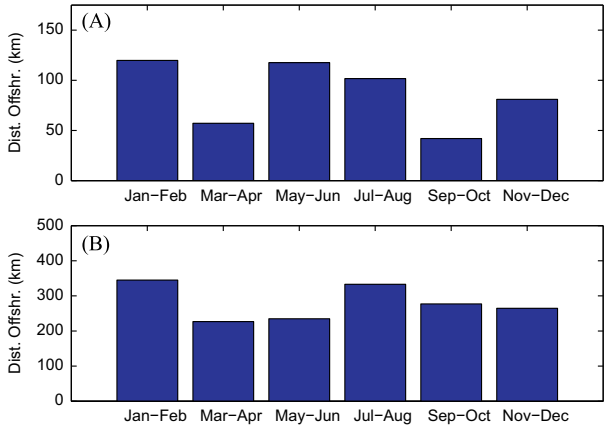

Fig. 6. Median distance of positive density fronts from shore along (A) line 80 and (B) line 90 during bi-monthly periods throughout the year.

3.4. Enhanced MVBS at ocean density fronts

The covariability of MVBS gradients with density gradients suggests that ocean fronts often function as borders between water parcels with differing zooplankton characteristics, indicating that denser surface waters on average either contain greater zooplankton biomass or contain zooplankton assemblages with different backscattering characteristics. The acoustic backscatter enhancement index associated with dives identified as positive density fronts (*i.e.*, inshore density > offshore density) is significantly elevated compared to all other, non-front dives (Fig. 9A and B; line 80: $p < 0.001$; line 90: $p < 0.001$, Mann–Whitney U test), whereas negative density fronts (*i.e.*, inshore density < offshore density) exhibited more negative enhancement index values compared with non-front dives (Fig. 9C and D; line 80: $p < 0.001$; line 90: $p < 0.001$). Positive density fronts were also associated with a positive Chl-*a* fluorescence enhancement index (Fig. 10A and B; line 80: $p < 0.001$; line 90: $p < 0.001$), whereas negative density fronts exhibited a negative Chl-*a* fluorescence enhancement index (Fig. 10C and D; line 80: $p < 0.001$; line 90: $p < 0.001$), indicating less Chl-*a* at that location. Together these results indicate that fronts not only act as borders between water parcels, but also that fronts can act as zones of biological enhancement. Instances of positive, negative, and zero enhancement at fronts did not show a clear pattern in seasonal or cross-shore distributions (Fig. 11).

3.5. Covariability of MVBS and MVBS gradients with other hydrographic variables

Other hydrographic variables in addition to density (temperature, salinity, SFU, spice, and horizontal velocities) and the respective horizontal gradients in these variables show significant relationships with mean surface MVBS and surface MVBS gradients, respectively (Table 1). While mean surface density and horizontal gradients in surface density remain the best predictors for mean surface MVBS and horizontal gradients in surface MVBS, respectively, temperature and temperature gradients are nearly as good predictors. Cross-track currents (v) and shear (dv/dx) were significantly correlated with MVBS and MVBS gradients, but the

Please cite this article as: Powell, J.R., Ohman, M.D., Covariability of zooplankton gradients with glider-detected density fronts in the Southern California Current System. Deep-Sea Res. II (2014), http://dx.doi.org/10.1016/j.dsr2.2014.04.002

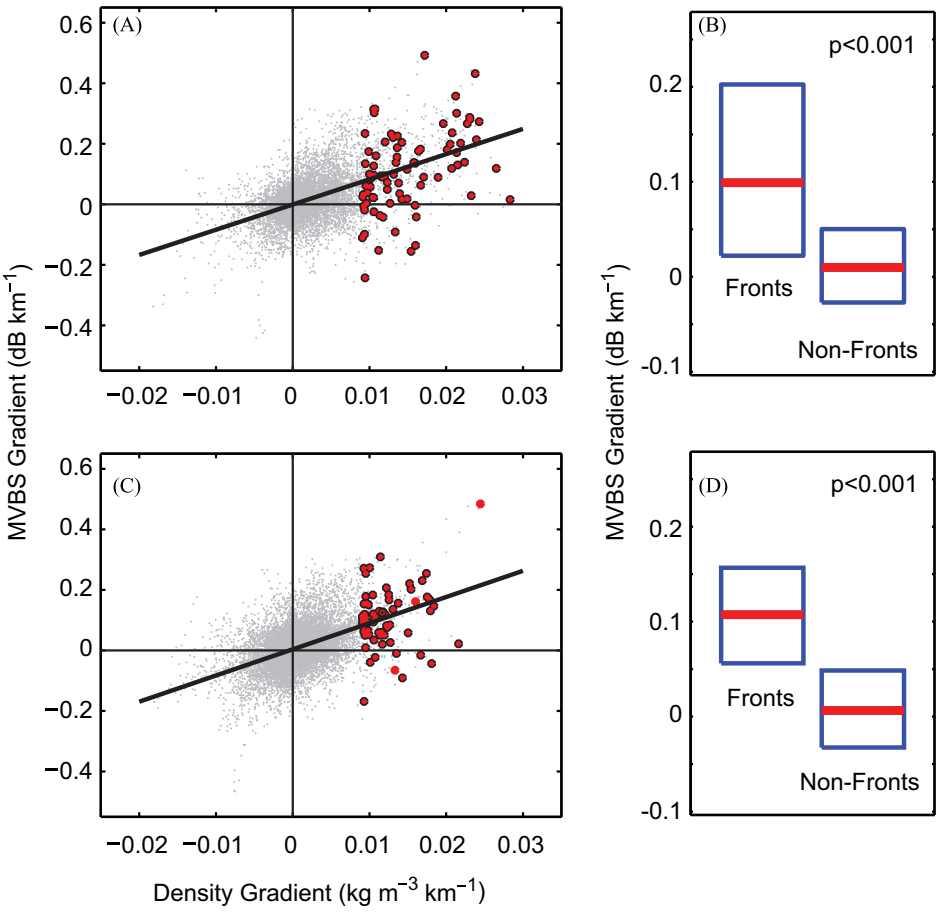

Fig. 7. Covariability of horizontal gradients in acoustic backscatter (MVBS) and seawater density for (A and B) line 80 and (C and D) line 90 at fronts and non-frontal regions. Gray points in the scatterplots indicate all dives and dark points are dives identified as positive density fronts. Boxplots compare median MVBS gradients in regions defined as fronts with MVBS gradients in non-frontal regions. Symbols for boxplots as in Fig. 5.

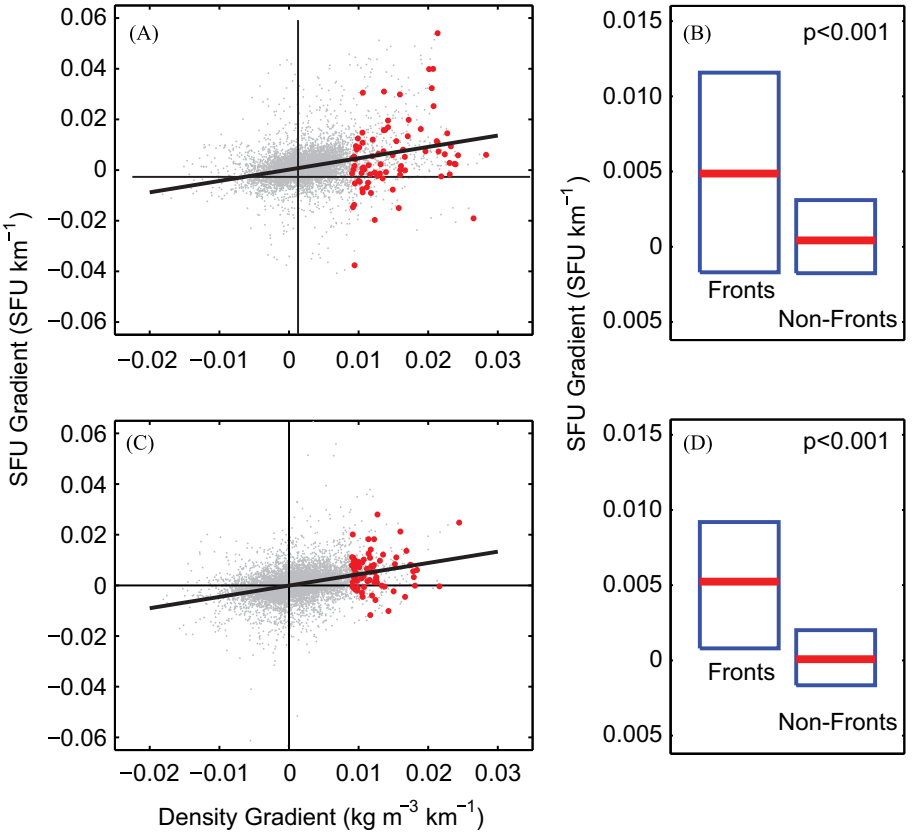

Fig. 8. Covariability of horizontal gradients in Chlorophyll-*a* fluorescence (as Standard Fluorescence Units, SFU) and seawater density for (A and B) line 80 and (C and D) line 90, at fronts and non-frontal regions. Boxplots compare median SFU gradients in regions defined as positive fronts with SFU gradients in non-frontal regions. Symbols for boxplots as in Fig. 5.

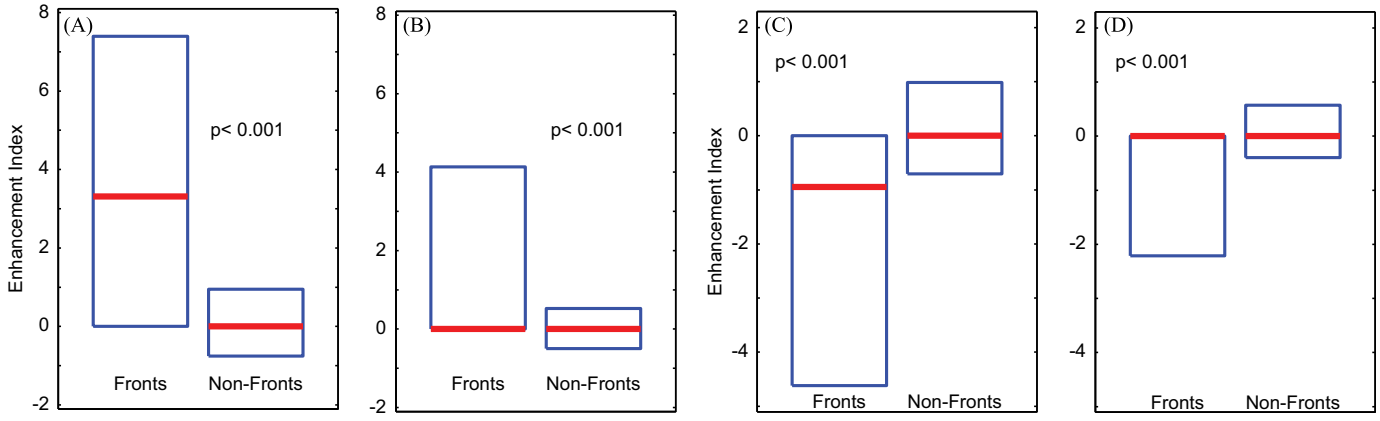

Fig. 9. (A and C) Line 80 and (B and D) line 90 acoustic backscatter (MVBS) Enhancement Index in relation to fronts. (A and B) Compare the enhancement index at fronts *vs.* non-fronts in regions of positive density fronts (*i.e.*, where inshore density > offshore density). (C and D) Compare the enhancement index in regions of negative density fronts (*i.e.*, where offshore density > inshore density). Symbols for boxplots as in Fig. 5.

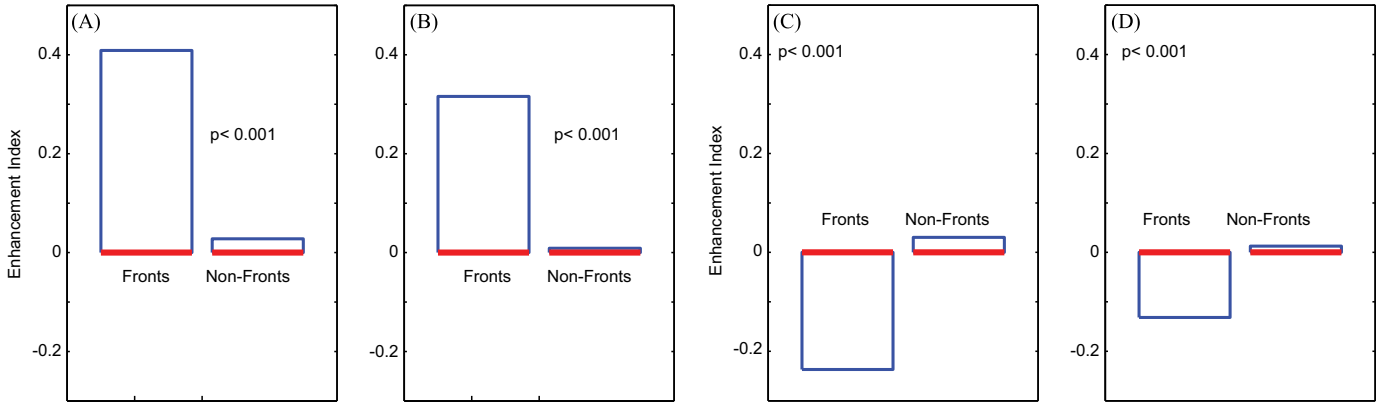

Fig. 10. (A and C) Line 80 and (B and D) line 90 Chl-*a* Fluorescence enhancement index in relation to fronts. (A and B) Compare the enhancement index (EI) at fronts *vs.* non-fronts in regions of positive density fronts (*i.e.*, where inshore density > offshore density). (C and D) compare the EI in regions of negative density fronts (*i.e.*, where offshore density > inshore density). Despite medians of zero over all profiles, EI exhibited enhancement (increased values) at positive fronts and dimunition (negative values) at negative fronts ($p < 0.001$, Mann–Whitney *U* test). Symbols for boxplots as in Fig. 5.

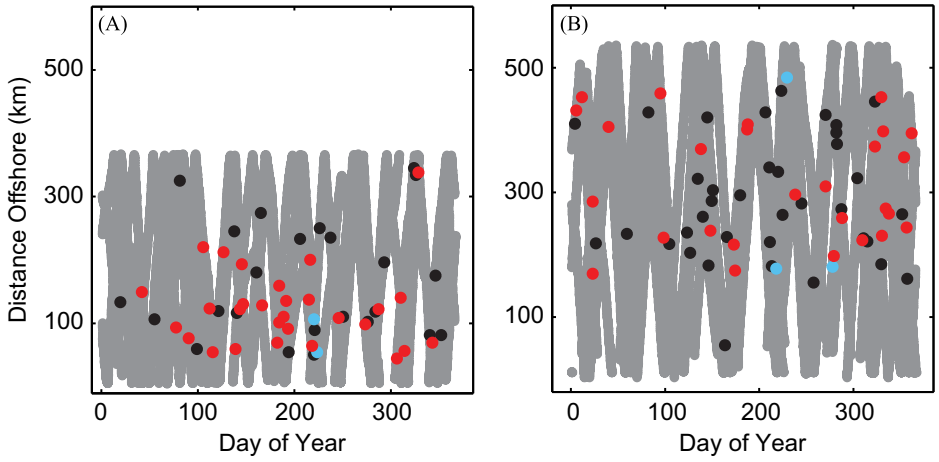

Fig. 11. Acoustic backscatter (MVBS) Enhancement Index at positive density fronts for (A) line 80, and (B) line 90. Red, blue and black dots indicate positive, negative and zero enhancement, respectively, at glider dives associated with positive density fronts. Gray dots indicate non-front dives. There are fewer points in this figure than in Fig. 4 because the Enhancement Index requires data for two 24-h periods inshore of a front.

relationship explained appreciable variance only for v along line 80. Along-track currents (u) and dilation (du/dx) showed weak or no correlations with MVBS or MVBS gradients.

Glider dives identified as density fronts showed stronger MVBS gradients than MVBS gradients at non-frontal dives ($p < 0.001$, Mann–Whitney *U* test). The median value of MVBS gradients at front dives was equal to the 88.1th percentile (along line 80) and 91.8th percentile (along line 90) of the MVBS gradients of non-front dives (Table 2). Again, other front types, particularly temperature, salinity, and SFU fronts, exhibited MVBS gradients that

Table 1
Spearman's rank correlation (r_s) of hydrographic and biotic variables and their respective gradients with Mean Volume Acoustic Backscatter (MVBS) and MVBS gradients.

Variable type	Line 80		Line 90	
	Mean, r_s	Gradient, r_s	Mean, r_s	Gradient, r_s
Density	0.73	0.42	0.60	0.43
Temperature	−0.69	−0.31	−0.53	−0.33
Salinity	0.45	0.28	0.42	0.22
Chl-*a*	0.51	0.23	0.48	0.26
Spice	−0.48	−0.06	−0.30	−0.17
Cross-track current (*v*)	0.37	0.09	0.04	−0.05
Along-track current (*u*)	−0.06	0.01*	−0.19	−0.13

* Indicates the correlation that is not significant ($p > 0.05$).

Table 2
Comparison of median Mean Volume Acoustic Backscatter (MVBS) gradients at hydrographic or biotic fronts *vs*. non-frontal regions, along lines 80 and 90. *p*-Values indicate significance of a Mann–Whitney *U* test. Percentile differential indicates the magnitude of the difference in median values of MVBS gradients at hydrographic or biotic frontal dives in comparison with non-frontal dives.

Front type	Line 80			Line 90		
	Median MVBS gradients differ?	*p*-Value	Percentile differential	Median MVBS gradients differ?	*p*-Value	Percentile differential
Density	Yes	< 0.001	38.1	Yes	< 0.001	41.8
Temperature	Yes	< 0.001	28.5	Yes	< 0.001	29.4
Salinity	Yes	< 0.001	38.1	Yes	< 0.001	32.5
Chl-*a*	Yes	< 0.001	30.7	Yes	< 0.001	28.4
Spice	Yes	0.005	16.7	Yes	0.029	7.4
$\partial v/\partial x$	No	0.356	6.9	No	0.502	7.1
$\partial u/\partial x$	Yes	0.011	10.7	Yes	0.003	13.6

differed significantly from non-front associated MVBS gradients (Table 2). The median MVBS gradient values at shear (dv/dx) fronts were not significantly different from the median MVBS gradient at non-front dives, ($p > 0.10$), while MVBS gradients were significantly ($p < 0.05$), but weakly enhanced at dilation (du/dx) fronts (Table 2).

4. Discussion

The high spatial resolution glider data, collected over six years, made it possible to address three questions concerning the coincidence of physical and biotic gradients. The results reveal, first, that open ocean density fronts in the Southern California Current System (SCCS) exhibit a non-random cross-shore distribution and, in the case of line 80, seasonality of occurrence. Second, horizontal gradients in acoustic backscatter (MVBS) and Chl-*a* are typically colocated with physical fronts. Third, fronts are more likely to be zones of plankton accumulation than non-frontal areas.

While each glider transect provides only a two-dimensional slice of a complex three-dimensional flow field, the existence of a multi-year collection of glider transects provided a series of repeated observations that made it possible to identify robust patterns between ocean fronts and plankton distributions. Analyses of the glider data suggest that the formation of biotic fronts and the accumulation of plankton are complex processes that cannot be attributed to a single causal mechanism. For example, Acoustic Doppler velocity data showed no consistent correlation with the presence of biotic fronts or accumulation zones, indicating that advective processes like convergence or horizontal shear were unlikely to be the sole mechanism responsible for their formation, although they could influence the formation of individual fronts. It also seems improbable that *in situ* growth can account solely for stronger MVBS gradients and accumulation observed at these fronts, since the generation time of the zooplankton taxa likely to contribute to the elevated MVBS is on the order of weeks to months, longer than most frontal conditions are likely to persist. However, it is conceivable that phytoplankton could accumulate within fronts in response to growth triggered by upwelled nutrients. It is also possible that alterations of zooplankton depth-seeking behaviors at fronts could lead to localized retention, but it is not possible to assess this hypothesis directly with the available data. It seems likely that zooplankton and phytoplankton accumulation zones form as the result of a combination of convergence, horizontal shear, altered growth rates, and behaviors. Directed studies are needed to examine the relative contributions of these mechanisms to biotic front formation in the SCCS. For example, additional gliders could repeatedly sample individual fronts identified by the line-transiting gliders in order to observe time-dependent flow fields, or gliders could carry additional biologically focused sensors that measure the potential for *in situ* growth (*e.g.*, nitrate sensors, or fast repetition rate fluorometers to ascertain the physiological state of phytoplankton).

The present paper directly compares hydrographic gradients in the upper ocean (50–0 m) layer with acoustic backscatter gradients and Chl-*a* fluorescence gradients. In our initial exploration of the data, it became clear that hydrographic and biotic variables in the upper ocean were better correlated than any combination of surface with subsurface measurements, or subsurface with subsurface measurements. A subsequent paper (Powell and Ohman, in review) that addresses differing plankton characteristics on either side of fronts, rather than the gradient region itself, includes analysis of subsurface responses.

Most studies of plankton responses to fronts have focused on predictable, recurrent shallow water features such as tidal and estuarine fronts (Pingree et al., 1975), or semi-permanent deep ocean fronts such as the Ligurian Front in the Mediterranean Sea (Boucher et al., 1987). In contrast, the Southern California Current System (SCCS) is characterized by complex and varying mesoscale structures including fronts, jets, and eddies, especially within a transitional zone centered

approximately 150–200 km offshore that separates the nearshore, coastally-upwelled waters from both the core California Current and from the subtropical-influenced waters further offshore (Lynn and Simpson, 1987). Modeling studies have suggested that intensification of equatorward winds, especially off central California, in spring and summer increase baroclinic instabilities in the wind-forced alongshore currents and consequently lead to an increase in frontogenesis with increased formation of meanders, jets, and mesoscale eddies (Capet et al., 2008; Marchesiello et al., 2003). Submesoscale and fine-scale frontal features can also be spawned from instabilities in the mesoscale features *via* ageostrophic secondary circulation (Johnston et al., 2011).

The present observations of the spatial and seasonal distribution of physical fronts are consistent with findings from other studies in the SCCS. In an analysis of ship-observed dynamic height anomalies, Lynn and Simpson (1987) found that the strongest cross-shore gradients in dynamic height occur during spring and summer, while the weakest cross-shore gradients occur during the winter months. Along line 80 especially, the glider observations suggest that fronts are fewer and perhaps somewhat weaker during the winter months. Lynn and Simpson (1987) further found that variability in dynamic height is greatest in a broad transitional zone centered approximately 200 km offshore along line 80 and 300 km offshore along line 90.

As the maximum gradients in dynamic height migrate offshore through the spring, summer, and fall, it would be reasonable to assume that conditions meeting the present front criteria would also match this seasonal progression and be seen in the seasonal and cross-shore distributions of glider-observed density fronts. However, fronts along line 80 consistently were most common closer to shore throughout the year, probably related to intermittent coastal upwelling and accompanying offshore Ekman transport in the vicinity of Pt. Conception. Fronts along line 90 more closely matched the expected progression, with front occurrence increasing from a minimum during March to April. Front incidence along line 90 was also maximal within the 150–300 km band from shore, again matching dynamic height data. Although that offshore region can also experience wind stress curl (Rykaczewski and Checkley, 2008), the presence of fronts in the region in autumn suggests that curl-driven upwelling gradients are not sufficient to explain the frontal occurrence. We find it noteworthy that the region of maximal front frequency along line 90 corresponds to a zone of enhanced mixing associated with submarine bottom topography along the Santa Rosa-Cortes Ridge (Fig. 1; cf. Johnston and Rudnick, in press). Frontal gradients would be expected to be elevated at both the offshore and inshore boundaries of this mixing zone.

Satellite altimetry data (Strub and James, 2000) also corroborate the seasonal distribution of fronts detected by gliders. Strub and James (2000) found that high eddy kinetic energy (EKE) first appears in the spring near the coast; as the year progresses, the zone of highest EKE moves offshore until winter when the California Current jet collapses and generally weak EKE is present. The seasonal progression in distance offshore of glider-detected fronts matches these observations, with the fewest fronts detected in winter months and the median distance offshore increasing from a minimum during the March to April period. The data hint that January–February months exhibited the greatest median distance offshore for fronts, which is consistent with the suggestion that a combination of generally weak EKE and few fronts leads to a more random distribution of fronts spread across the entire cross-shore range.

The glider data are also partially corroborated by a study of the seasonality of satellite-detected thermal fronts in the CCS (Castelao et al., 2006), which measured the bi-monthly climatology of the magnitude of thermal gradients as well as the cross-shore probability distribution of front occurrence from 2001 to 2004. Similar to the glider results presented here, Castelao et al. (2006) found that the winter months were marked by fewer and weaker fronts that were broadly distributed cross-shore, followed by an abrupt shift to more numerous and stronger fronts that were concentrated in the nearshore in the March–April period. After March and April, the zone of strong fronts and high front probability migrated farther offshore. This progression is similar to that observed by gliders along line 90, but is not clearly observable in the line 80 data. Since the glider observations do not overlap in time with the satellite observations, it is unclear whether interannual variation in seasonal patterns would explain the observed differences. However, the magnitude of temperature gradients at the satellite-detected thermal fronts closely matched those measured at glider-detected fronts, suggesting that the fronts detected in the Castelao study may represent the same phenomena as those measured by the glider. Kahru et al. (2012) also found a similar seasonal pattern in satellite-detected thermal front frequency in the waters north of Point Conception, with the fewest fronts occurring in winter followed by steadily increasing frontal frequencies throughout the spring and summer.

Seasonally and spatially varying patterns of hydrographic fronts in the CCS contribute to heterogeneous distributions of food resources in the region, which likely have important consequences for herbivorous and carnivorous animals. Mullin and Brooks (1976) observed that most zooplankton would likely starve if food was uniformly distributed throughout the ocean. For both mobile planktivores and for zooplankton that might alter their vertical migration behavior to increase retention in fronts, the observed enhancement of potential food resources at fronts could represent an important foraging opportunity. Thus, the results presented here demonstrating that both Chl-*a* fluorescence gradients and MVBS gradients covary with hydrographic gradients during an extended sampling period and over a wide geographic area are important for several reasons. First, both satellite-based observational studies and modeling studies have demonstrated that open ocean fronts are a common feature in the ocean, especially in Eastern Boundary Upwelling Ecosystems such as the CCS (Belkin et al., 2009). Seasonal changes in the distribution of fronts (and therefore potentially the seasonal changes in food availability) may influence the timing of reproduction, feeding, and migration strategies for many species.

Second, the demonstrated covariability of physical and biological gradients complements observations that mobile predators like tuna target frontal regions (Fiedler and Bernard, 1987; Laurs et al., 1984; Sund et al., 1981). Given that there is increased likelihood of potential prey at these locations, the ability of a predator to swim up gradients would be an adaptive trait. Foraging strategies of mobile predators are not well understood, and it is unclear whether predators follow physical (*e.g.*, temperature) gradients or gradients of prey concentration. The present results at least suggest that following physical gradients alone could be a successful strategy.

Third, given the glider data presented here, we can estimate a mobile predator's success rate in locating waters with better foraging potential if they were to travel up horizontal density gradients. As Fig. 12 demonstrates, mobile predators traveling up a strong density gradient, such as would be found in a frontal zone, will encounter waters with higher mean acoustic backscatter (implying higher zooplankton densities) approximately 85% of the time, while a mobile predator traveling down this density gradient would find richer waters only 15% of the time. These foraging success rates are independent of whether the predator is moving inshore or offshore. Thus, there would seem to be a strong selective pressure for mobile predators to preferentially travel up density gradients.

Please cite this article as: Powell, J.R., Ohman, M.D., Covariability of zooplankton gradients with glider-detected density fronts in the Southern California Current System. Deep-Sea Res. II (2014), http://dx.doi.org/10.1016/j.dsr2.2014.04.002

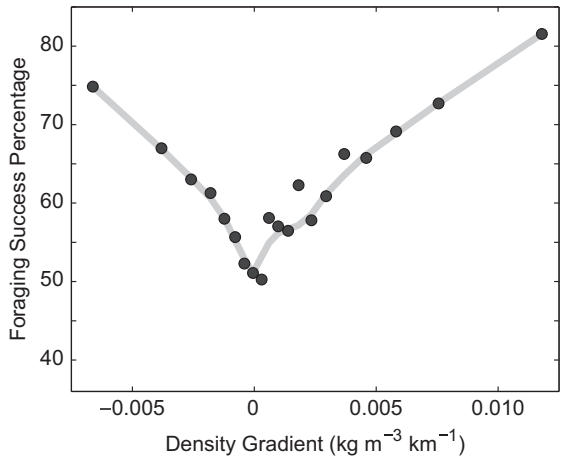

Fig. 12. Percent chance of a mobile predator locating waters with higher mean acoustic backscatter (MVBS) by migrating up a local density gradient. Positive density gradients indicate that the waters inshore of the location are denser than offshore while negative density gradients are the opposite. The gray line is a Loess smoother.

Additionally, strictly physical accumulation mechanisms that entrain and concentrate plankton within frontal zones could have other important ecological effects such as stimulating rates of zooplankton grazing on phytoplankton, zooplankton mate encounter, reproductive success and fecundity, and somatic growth. Population dynamics may be significantly altered at fronts compared to non-frontal zones.

A recent analysis of satellite data found a long-term increase in the frequency of satellite-detected Chl-*a* and SST fronts within a 110,000 km^2 study area in the SCCS (Kahru et al., 2012). The frequency of SST fronts increased almost 35% between 1981 and 2011, while the frequency of Chl-*a* fronts increased over 50% between 1997 and 2011. Kahru et al. (2012) attributed the increased frequency of fronts to the increased incidence of filaments and eddies driven by an increase in upwelling-favorable winds and coastal upwelling during the period (García-Reyes and Largier, 2010). Since ocean models of a warming SCCS project an intensification of mean currents and increased mesoscale eddy variance (Di Lorenzo et al., 2005), it seems likely that the frequency of fronts, and their importance to pelagic organisms, will continue to increase in the future.

Acknowledgments

We gratefully acknowledge Russ Davis, Dan Rudnick, Robert Todd, and Jeff Sherman for the provision of *Spray* glider data and for their advice on glider instrumentation and technical issues. Russ Davis, Peter Franks, Mike Landry, and the anonymous reviewers provided important feedback on the manuscript. The funding for this work was provided by NSF *via* the California Current Ecosystem LTER site, and by the Gordon and Betty Moore Foundation.

References

Ainley, D.G., Dugger, K.D., Ford, R.G., Pierce, S.D., Reese, D.C., Brodeur, R.D., Tynan, C. T., Barth, J.A., 2009. Association of predators and prey at frontal features in the California Current: competition, facilitation, and co-occurrence. Mar. Ecol. Prog. Ser. 389, 271–294, http://dx.doi.org/10.3354/Meps08153.

Belkin, I.M., Cornillon, P.C., Sherman, K., 2009. Fronts in large marine ecosystems. Prog. Oceanogr. 81, 223–236, http://dx.doi.org/10.1016/j.pocean.2009.04.015.

Bost, C.A., Cotte, C., Bailleul, F., Cherel, Y., Charrassin, J.B., Guinet, C., Ainley, D.G., Weimerskirch, H., 2009. The importance of oceanographic fronts to marine birds and mammals of the southern oceans. J. Mar. Syst. 78, 363–376, http://dx.doi.org/10.1016/j.jmarsys.2008.11.022.

Boucher, J., Ibanez, F., Prieur, L., 1987. Daily and seasonal-variations in the spatial-distribution of zooplankton populations in relation to the physical structure in the Ligurian Sea Front. J. Mar. Res. 45, 133–173.

Bower, A.S., 1991. A simple kinematic mechanism for mixing fluid parcels across a meandering jet. J. Phys. Oceanogr. 21, 173–180.

Capet, X., McWilliams, J.C., Molemaker, M.J., Shchepetkin, A.F., 2008. Mesoscale to submesoscale transition in the California current system. Part II: frontal processes. J. Phys. Oceanogr. 38, 44–64, http://dx.doi.org/10.1175/2007jpo3672.1.

Castelao, R.M., Mavor, T.P., Barth, J.A., Breaker, L.C., 2006. Sea surface temperature fronts in the California Current System from geostationary satellite observations. J. Geophys. Res. Oceans 111, C09026, http://dx.doi.org/10.1029/2006jc003541.

Claustre, H., Kerherve, P., Marty, J.C., Prieur, L., Videau, C., Hecq, J.H., 1994. Phytoplankton dynamics associated with a geostrophic front: ecological and biogeochemical implications. J. Mar. Res. 52, 711–742, http://dx.doi.org/10.1357/0022240943077000.

Cullen, J.J., Lewis, M.R., 1995. Biological processes and optical measurements near the sea surface: some issues relevant to remote sensing. J. Geophys. Res. Oceans 100, 13255–13266, http://dx.doi.org/10.1029/95jc00454.

D'Asaro, E., Lee, C., Rainville, L., Harcourt, R., Thomas, L., 2011. Enhanced turbulence and energy dissipation at ocean fronts. Science 332, 318–322, http://dx.doi.org/10.1126/science.1201515.

Davis, R.E., Ohman, M.D., Rudnick, D.L., Sherman, J.T., Hodges, B., 2008. Glider surveillance of physics and biology in the southern California Current System. Limnol. Oceanogr. 53, 2151–2168.

Di Lorenzo, E., Miller, A.J., Schneider, N., McWilliams, J.C., 2005. The warming of the California Current system: dynamics and ecosystem implications. J. Phys. Oceanogr. 35, 336–362.

Fiedler, P.C., Bernard, H.J., 1987. Tuna aggregation and feeding near fronts observed in satellite imagery. Cont. Shelf Res. 7, 871–881, http://dx.doi.org/10.1016/0278-4343(87)90003-3.

Flament, P., 2002. A state variable for characterizing water masses and their diffusive stability: spiciness. Prog. Oceanogr. 54, 493–501, http://dx.doi.org/10.1016/s0079-6611(02)00065-4.

Franks, P.J.S., 1992. Sink or swim – accumulation of biomass at fronts. Mar. Ecol. Prog. Ser. 82, 1–12.

Franks, P.J.S., Walstad, L.J., 1997. Phytoplankton patches at fronts: a model of formation and response to wind events. J. Mar. Res. 55, 1–29, http://dx.doi.org/10.1357/0022240973224472.

García-Reyes, M., Largier, J., 2010. Observations of increased wind-driven coastal upwelling off central California. J. Geophys. Res. 115, C04011, http://dx.doi.org/10.1029/2009JC005576.

Haury, L.R., Venrick, E.L., Fey, C.L., McGowan, J.A., Niiler, P.P., 1993. The Ensenada Front: July 1995. Calif. Coop.Ocean. Fish. Investig. Rep. 34, 69–88.

Johnston, T.M.S., Rudnick, D.L., Trapped diurnal internal tides, propagating semi-diurnal internal tides, and mixing estimates in the California Current System from sustained glider observations, 2006–2012. Deep-Sea Res. II. http://dx.doi.org/10.1016/j.dsr2.2014.03.009 this issue.

Johnston, T.M.S., Rudnick, D.L., Pallas-Sanz, E., 2011. Elevated mixing at a front. J. Geophys. Res. Oceans, 116, http://dx.doi.org/10.1029/2011jc007192.

Kahru, M., Di Lorenzo, E., Manzano-Sarabia, M., Mitchell, B.G., 2012. Spatial and temporal statistics of sea surface temperature and chlorophyll fronts in the California Current. J. Plankton Res. 34, 749–760, http://dx.doi.org/10.1093/plankt/fbs010.

Kai, E.T., Rossi, V., Sudre, J., Weimerskirch, H., Lopez, C., Hernandez-Garcia, E., Marsac, F., Garcon, V., 2009. Top marine predators track Lagrangian coherent structures. Proc. Natl. Acad. Sci. USA 106, 8245–8250, http://dx.doi.org/10.1073/pnas.0811034106.

Landry, M.R., Ohman, M.D., Goericke, R., Stukel, M.R., Barbeau, K.A., Bundy, R., Kahru, M., 2012. Pelagic community responses to a deep-water front in the California Current Ecosystem: overview of the A-front study. J. Plankton Res. 34, 739–748, http://dx.doi.org/10.1093/plankt/fbs025.

Laurs, R.M., Fiedler, P.C., Montgomery, D.R., 1984. Albacore tuna catch distributions relative to environmental features observed from satellites. Deep-Sea Res. 31, 1085–1099.

Lefevre, J., 1986. Aspects of the biology of frontal systems. Adv. Mar. Biol. 23, 163–299.

Legeckis, R., 1978. Survey of worldwide sea-surface temperature fronts detected by environmental satellites. J. Geophys. Res. Oceans. Atmos. 83, 4501–4522, http://dx.doi.org/10.1029/JC083iC09p04501.

Lynn, R.J., Simpson, J.J., 1987. The California Current System – the seasonal variability of its physical characteristics. J. Geophys. Res. Oceans 92, 12947–-12966, http://dx.doi.org/10.1029/Jc092ic12p12947.

Mackas, D.L., Washburn, L., Smith, S.L., 1991. Zooplankton community pattern associated with a California Current cold filament. J. Geophys. Res. Oceans 96, 14781–14797.

Marchesiello, P., McWilliams, J.C., Shchepetkin, A., 2003. Equilibrium structure and dynamics of the California Current System. J. Phys. Oceanogr. 33, 753–783, http://dx.doi.org/10.1175/1520-0485(2003)33<753:esadot>2.0.co;2.

Medwin, H., Clay, C.S., 1998. Fundamentals of Acoustical Oceanography. Academic Press, Boston.

Moser, H.G., Smith, P.E., 1993. Larval fish assemblages of the California Current region and their horizontal and vertical distributions across a front. Bull. Mar. Sci. 53, 645–691.

Mullin, M.M., Brooks, E.R., 1976. Some consequences of distributional heterogeneity of phytoplankton and zooplankton. Limnol. Oceanogr. 21, 784–796.

Ohman, M.D., Powell, J.R., Picheral, M., Jensen, D.W., 2012. Mesozooplankton and particulate matter responses to a deep-water frontal system in the southern

California Current System. J. Plankton Res. 34, 815–827, http://dx.doi.org/10.1093/plankt/fbs028.
Ohman, M.D., Rudnick, D.L., Chekalyuk, A., Davis, R.E., Feely, R.A., Kahru, M., Kim, H.-J., Landry, M.R., Martz, T.R., Sabine, C., Send, U., 2013. Autonomous ocean measurements in the California Current Ecosystem. Oceanography 26, 18–25, http://dx.doi.org/10.5670/oceanog.2013.41.
Pingree, R.D., Pugh, P.R., Holligan, P.M., Forster, G.R., 1975. Summer phytoplankton blooms and red tides along tidal fronts in approaches to english channel. Nature 258, 672–677, http://dx.doi.org/10.1038/258672a0.
Podesta, G.P., Browder, J.A., Hoey, J.J., 1993. exploring the association between swordfish catch rates and thermal fronts on United States longline grounds in the western North Atlantic. Cont. Shelf Res. 13, 253–277, http://dx.doi.org/10.1016/0278-4343(93)90109-B.
Powell, J.R., Ohman, M.D., 2012. Use of glider-class acoustic Doppler profilers for estimating zooplankton biomass. J. Plankton Res. 34, 563–568, http://dx.doi.org/10.1093/plankt/fbs023.
Powell, J.R., Ohman, M.D. Changes in zooplankton habitat, behavior, and acoustic scattering characteristics across glider-detected density fronts in the Southern California Current System, Prog. Oceanogr., in review.
Rykaczewski, R.R., Checkley Jr., D.M., 2008. Influence of ocean winds on the pelagic ecosystem in upwelling regions. Proc. Natl. Acad. Sci. USA 105, 1965–1970.
Sherman, J., Davis, R.E., Owens, W.B., Valdes, J., 2001. The autonomous underwater glider "Spray". IEEE J. Ocean. Eng. 26, 437–446.
Smith, S.L., Lane, P.V.Z., 1991. The jet off Point Arena, California: its role in aspects of secondary production in the copepod *Eucalanus californicus* Johnson. J. Geophys. Res. Oceans 96, 14849–14858.
SonTek, 1997. SonTek Doppler current meters: using signal strength data to monitor suspended sediment concentration. Application Note, pp. 1–7.
Sournia, A., 1994. Pelagic biogeography and fronts. Prog. Oceanogr. 34, 109–120.
Strub, P.T., James, C., 2000. Altimeter-derived variability of surface velocities in the California Current System: 2. Seasonal circulation and eddy statistics. Deep-Sea Res. II 47, 831–870.
Sund, P.N., Blackburn, M., Williams, F., 1981. Tunas and their environment in the Pacific Ocean: a review. Oceanogr. Mar. Biol. Annu. Rev. 19, 443–512.
Taylor, A.G., Goericke, R., Landry, M.R., Selph, K.E., Wick, D.A., Roadman, M.J., 2012. Sharp gradients in phytoplankton community structure across a frontal zone in the California Current Ecosystem. J. Plankton Res. 34, 778–789, http://dx.doi.org/10.1093/plankt/fbs036.
Tynan, C.T., Ainley, D.G., Barth, J.A., Cowles, T.J., Pierce, S.D., Spear, L.B., 2005. Cetacean distributions relative to ocean processes in the northern California Current System. Deep-Sea Res. II 52, 145–167, http://dx.doi.org/10.1016/j.dsr2.2004.09.024.

Please cite this article as: Powell, J.R., Ohman, M.D., Covariability of zooplankton gradients with glider-detected density fronts in the Southern California Current System. Deep-Sea Res. II (2014), http://dx.doi.org/10.1016/j.dsr2.2014.04.002